Strong, tough and environment-tolerant organohydrogels for flaw-insensitive strain sensing

Yuqing Wang[1], Zhanqi Liu[1], Yuntao Liu[1], Jun Yan[1], Haidi Wu[1], Hechuan Zhang[1], Huamin Li[1], Junjie Wang[1], Huaiguo Xue[1], Ling Wang[2], Yongqian Shi[3], Longcheng Tang[4], Pingan Song[5], Jiefeng Gao[1]*

[1] School of Chemistry and Chemical Engineering, Yangzhou University, No 180, Road Siwangting, Yangzhou, Jiangsu, 225002, China

[2] School of Chemistry and Chemical Engineering, Anqing Normal University, Anqing 246011, China

[3] College of Environment and Safety Engineering, Fuzhou University, Fuzhou 350116, China

[4] College of Material, Chemistry and Chemical Engineering, Key Laboratory of Organosilicon Chemistry and Material Technology of MoE, Key Laboratory of Silicone Materials Technology of Zhejiang Province, Hangzhou Normal University, Hangzhou 311121, China

[5] Centre for Future Materials, University of Southern Queensland, Springfield Campus, QLD 4300, Australia

*Corresponding author: E-mail address: jfgao@yzu.edu.cn

Abstract

Conductive organohydrogels are promising for strain sensing, while their weak mechanical properties, poor crack propagation resistance and unstable sensing signals during the long-term use have seriously limit their applications as high-performance strain sensors. Here, we propose a facile method, i.e., solvent exchange assisted hot-pressing, to prepare strong yet tough, transparent and anti-fatigue ionically conductive organohydrogels (ICOHs). The densified polymeric network and improved crystallinity endow ICOHs with excellent mechanical properties. The tensile strength, toughness, fracture energy and fatigue threshold of ICOHs can reach 36.12 ± 4.15 MPa, 54.57 ± 2.89 MJ/m^3, 43.44 ± 8.54 kJ/m^2 and 1212.86 ± 57.20 J/m^2, respectively, with a satisfactory fracture strain of 266 ± 33%. In addition, the ICOH strain sensors with freezing and drying resistance exhibit excellent cyclic stability (10,000 cycles). More importantly, the fatigue resistance allows the notched strain sensor to work normally with no crack propagation and output stable and reliable sensing signals. Overall, the unique flaw-insensitive strain sensing makes ICOHs promising in the field of wearable and durable electronics.

1. Introduction

Conducive organohydrogel (COHs) with flexibility and skin affinity show their unique advantages in freezing resistance, high water retention capability and thermal stability [1-5], by comparison with their counterpart hydrogels, and have been excellent candidates for wearable strain sensors [6-9]. Conductive nanofillers such as MXene [10, 11] and reduced graphene oxide [12] are usually incorporated into organohydrogels for preparation of electrically conducive organohydrogels [13]. Generally, high nanofiller concentration is required to form electrical percolation pathways, giving rise to a large percolation threshold as well as the reduced stretchability of COHs [14-16]. In addition, the aggregation of conductive nanofillers in COHs even at a low concentration would lead to the deterioration of mechanical properties and unstable sensing signals.

As an alternate, ionically conductive organohydrogel (ICOH) strain sensors have been developed, and the ions can be uniformly dispersed in the organohydrogels to form conductive network [17-22]. Much effort has been devoted to improving the mechanical properties of ICOH strain sensors to ensure their reliability and durability during practical use. Nanofillers such as polymer nanofibers are used to enhance the tensile strength and modulus of ICOHs [19]. For example, the MXene organohydrogels were prepared by directional freezing and solvent exchange, and the toughness of the conductive organohydrogel was significantly increased to 82 kJ/m^3 at the MXene concentration of 3 mg/ml, and the excessive concentration of MXene would lead to aggregation and degradation of mechanical properties [23]. Furthermore, mechanically robust ICOHs were prepared by a "water vapor assisted aramid nanofiber (ANF) reinforcement" method [24], and possessed the tensile strength, toughness and fatigue threshold of up to approximately 1.88 MPa, 6.75 MJ/m^3 and 328 J/m^2, respectively, with the ANF content of 0.15 wt %. Both uniform distribution and sufficient interfacial interaction between these nanofillers and macromolecular chains are indispensable for enhancing mechanical properties. Also, the nanofiller concentration should be controlled at a relatively low level to guarantee the proper solution viscosity and satisfactory dispersion, greatly limiting their improvement in mechanical properties. Furthermore, it remains challenging to balance the mechanical and ionically conductive properties in the organohydrogels.

As known, strain sensors usually need to undergo repeated mechanical deformations, and thus the cyclability and durability are highly desirable[25]. More importantly, the strain sensors should possess

excellent crack propagation resistance, so that they can work normally even when flaws or micro-cracks are generated inside the materials during multiple deformations. Otherwise, cracks may propagate quickly, leading to unstable sensing signals and even material failure in a short time. Despite the importance, the fatigue resistance for strain sensing of ICOHs receives little attention.

Here, we reported strong, transparent and anti-fatigue ICOHs through macromolecular chain aggregation induced densification of polymeric network for flaw-insensitive strain sensing. The tensile strength, toughness, fracture energy and fatigue threshold of ICOHs can reach 36.12 ± 4.15 MPa, 54.57 ± 2.89 MJ/m^3, 43.44 ± 8.54 kJ/m^2 and 1212.86 ± 57.20 J/m^2, respectively, with a satisfactory fracture strain of 266 ± 33%. Environmentally stable ICOH strain sensors with freezing resistance and thermal stability showed a quick response and excellent cyclability (10 000 cycles). Particularly, ICOHs possessed outstanding crack propagation resistance, and even the notched strain sensor can work normally with the stable and reliable sensing signal output in a wide range of temperatures, and the unique flaw-insensitive strain sensing made ICOHs promising in the field of high performance and durable electronics.

2. Results and Discussions

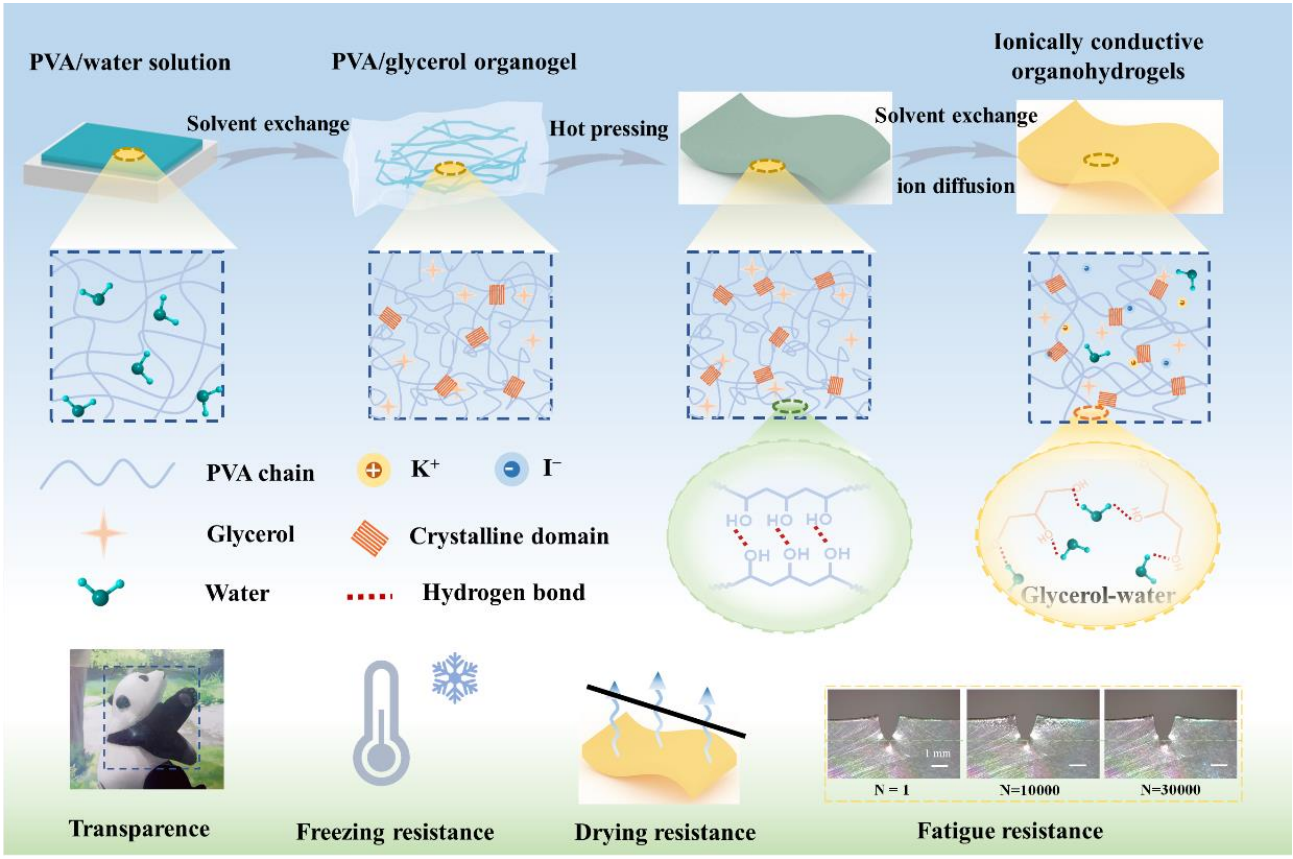

Figure 1. Schematic fabrication of the ionically conductive organohydrogel (ICOHs) through a solvent exchange assisted hot-pressing strategy.

Herein, as shown in Figure 1, ionically conductive organohydrogels (ICOHs) with high strength and fatigue resistance were prepared based on the synergy of solvent exchange and hot-pressing. As known, solvent exchange was an effective method for preparing strong PVA gels by regulating the conformation of polymer chains [26, 27]. PVA was firstly dissolved in water (a relatively good solvent) to form a uniform and transparent solution. At this time, PVA macromolecules were disentangled with an extended conformation due to their favorable interaction with water molecules through hydrogen bonding [28]. When the PVA solution was placed into glycerol, solvent exchange occurred, because water was miscible with glycerol. On the other hand, glycerol was a poor solvent for PVA, and hence PVA macromolecules tended to aggregate, forming numerous crystalline domains served as physical crosslinking points and thus constructing a strong polymer network in the organogel. Subsequently, the obtained PVA/glycerol organogels experienced hot-pressing, which further improved the crystallinity of PVA and at the same time promoted the densification of the polymeric network. Due to

the high boiling point of glycerol, PVA/glycerol organogel exhibited mechanical stability in the temperature range of 25~120 ℃ and maintained the structure integrity during hot-pressing. When the temperature reached 120 ℃, the storage modulus (*G*') began to decline and the loss modulus (*G*") gradually increased (Figure S1). Therefore, the mechanical properties of the organogels can be adjusted in a wide temperature range during hot pressing. Finally, ICOHs were obtained after the glycerol was completely replaced by KI/glycerol/water through two-step solvent exchange. The glycerol/water binary solvent is widely used as an anti-freezing and anti-drying medium, because the abundant hydrogen bonds between glycerol and water significantly decreases the vapor pressure of water, making evaporation difficult. Consequently, the environmental stability of the organohydrogels is greatly improved. On the other hand, the glycerol/water has limited solubility towards most inorganic salt ions especially at a relatively high glycerol content. Here, potassium iodide (KI) was chosen to construct the ionically conductive network in the organohydrogels, because it possessed good solubility in the mixed solvent of glycerol and water while brought no negative effect on the mechanical properties of the organohydrogels. Based on the synergistic effect of solvent exchange and hot pressing, the obtained organohydrogels had excellent mechanical properties. More importantly, the KI/glycerol/water solvent endowed the organohydrogels with ionic conductivity, anti-freezing and anti-drying properties, which laid a firm foundation for the application of anti-fatigue strain sensors.

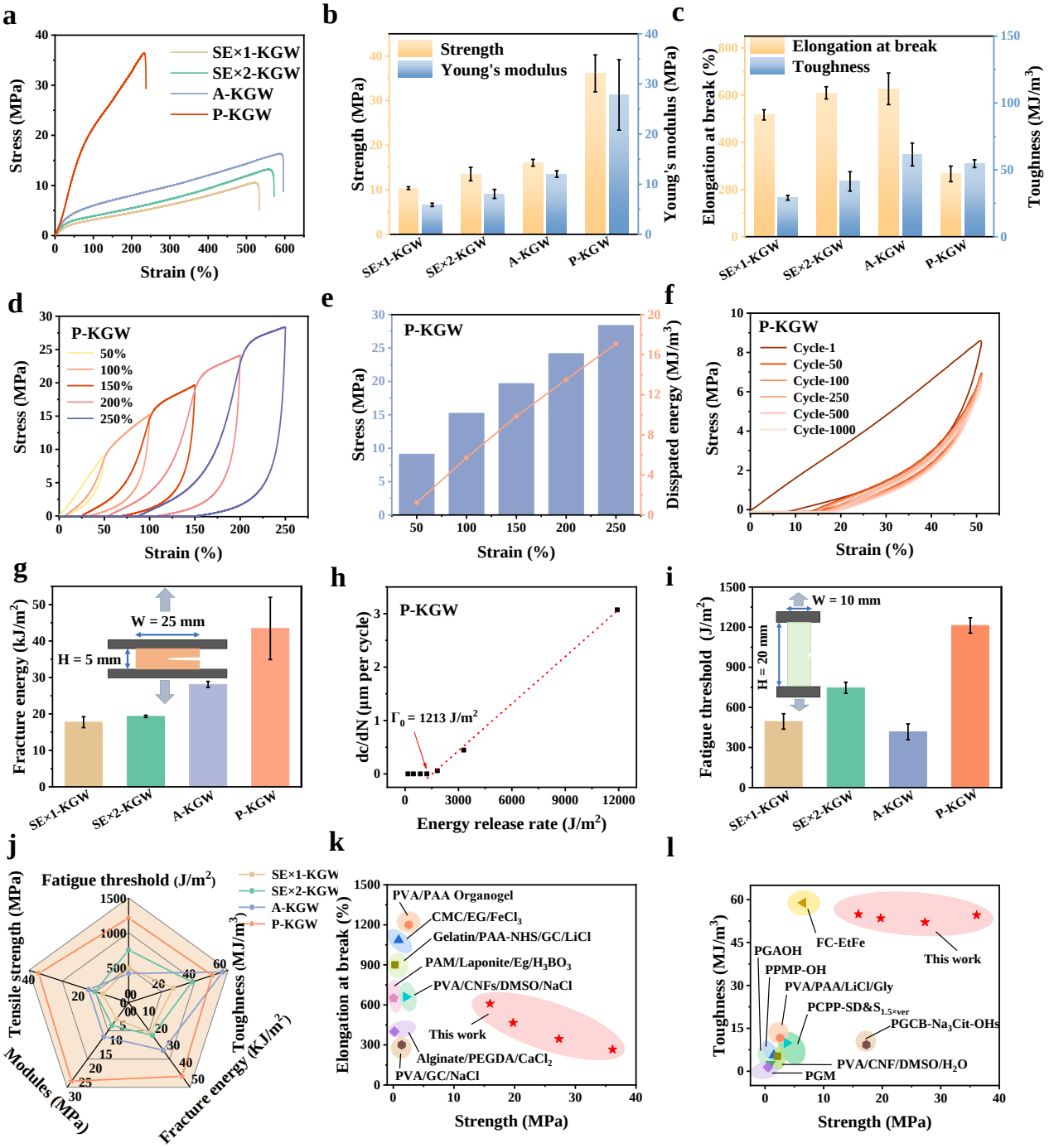

Figure 2. Mechanical properties of ICOHs. (a) Monotonic tensile stress-strain curves of different ICOHs, and the summary of (b) tensile strength and elongation at break and (c) Young's modules and toughness. (d) Sequential tensile loading-unloading tests under incremental strains and (e) its maximum stress and dissipated energy for P-KGW. (f) 1000 cycles of stretching-releasing curves at 50% strain for P-KGW. (g) fracture energy. (h) Crack propagation per cycle dc/dN versus applied energy release rate of P-KGW. (i) Fatigue threshold of different ICOHs. (j) The comparison of comprehensive mechanical properties of different ICOHs. (k-l) Comparison of mechanical properties of ICOs with those of other gel materials (PVA/PAA Organogel [5], $CMC/EG/FeCl_3$ [29], $Alginate/PEGDA/CaCl_2$ [17], PVA/CNFs/DMSO/NaCl [20], PVA/GC/NaCl [30], Gelatin/PAA-NHS/GC/LiCl [21], $PAM/Laponite/Eg/H_3BO_3$ [31], PVA/PAA/LiCl/Gly [5], PPMP-OH [8], PGAOH [7], PGM

[32], FC-EtFe [3], PCPP-SD&S$_{1.5\times ver}$ [33], PGCB-Na$_3$Cit-Ohs [34], PVA-CNF-DMSO-H$_2$O [20]).

For the convenience of description, the KI/glycerol/water (abbreviated as KGW) organohydrogels based on heat-cooling, one-step solvent exchange, two-step solvent exchange and wet annealing were named HC-KGW, SE×1-KGW, SE×2-KGW and A-KGW, respectively. In the test of mechanical properties, the tensile rate was set to 50 mm min^{-1} (with corresponding to strain rate of 2.5 min^{-1}). Uniaxial tensile test was performed to evaluate the contribution of solvent exchange and hot pressing to the mechanical properties of ICOHs (Figure 2a-c). The tensile strength and Young's modulus of the SE×1-KGW were 10.37 and 5.88 MPa, respectively, much higher than those of HC-KGW (0.12 and 0.23 MPa, respectively) (Figure S2). Two values were enhanced to 13.53 and 8.07 MPa for SE×2-KGW, indicating that the two-step solvent exchange can further regulate the conformation of the PVA macromolecular chains and form a more compact polymeric network. Hot-pressing can improve the mechanical properties of the organohydrogels, depending on the pressing temperature. It was found that hot-pressing at room temperature slightly increased strength and modulus of ICOHs. The tensile strength and Young's modulus of ICOHs increased with the increase of hot-pressing temperature, while the elongation at break gradually decreased and the toughness was almost unchanged (Figure S3). Organohydrogels at a hot pressing temperature of 120 ℃ (abbreviated as P$_{120}$-KGW) showed the highest strength and Young's modulus of 36.12 and 27.81 MPa, respectively, much higher than those of SE×2-KGW and A-KGW, reflecting the synergy of pressing and annealing on the improvement of mechanical properties of ICOHs. The effect of KI concentration on mechanical properties was also taken into account (Figure S4). The results showed that KI content hardly influence mechanical properties of ICOHs. KI can be easily dissolved in glycerol/water, and salt ions would not precipitate in the gel even at low temperatures. On the other hand, with the increase of KI concentration, the ionic conductivity increased from 0.96 mS/m for P$_{120}$-K$_5$GW to 12.5 mS/m for P$_{120}$-K$_{30}$GW (Figure S5). Therefore, P$_{120}$-K$_{30}$GW (abbreviated as P-KGW) was determined for subsequent characterization and sensing performance tests.

SE×1-KGW and P-KGW were stretched to 50% strain, held at 50% tensile strain for 10 min, and then recovered. The tensile set values of SE×1-KGW and P-KGW are 0.127 ± 0.010 and 0.098 ± 0.009 (Figure S6). This result verified the good elasticity of P-KGW. Cyclic loading and unloading with step increase of the strain (50%) was conducted to characterize the energy dissipation capacity of ICOHs. The maximum stress and dissipated energy increased with increasing tensile strain, and the dissipated

energy of P-KGW reached 17.08 MJ/m^3 with the maximum stress of 28.38 MPa at the tensile strain of 250% (Figure 2d-e, Figure S7). 1000 cyclic tensile loading and unloading tests at 50% strain were performed to verify the fatigue resistance of ICOHs (Figure 2f, Figure S8 and S9). The maximum stress of SE×1-KGW, SE×2-KGW, A-KGW, P-KGW during the first cycle was 2.45, 2.71, 5.79 and 8.59 MPa, respectively. As the number of cycles increased, the maximum stress and dissipation energy decreased. After 50 cycles, they reached equilibrium values. After 1000 cycles, the maximum stress and dissipation energy of P-KGW were 6.36 MPa and 87.46 kJ/m^3, respectively, 74% and 7% of those in the first cycle.

In practical use, crack resistance is highly important and can greatly affect material's service life. The crack-resistance of the material under a static load is also examined[35, 36]. With the increase of time under 10% tensile strain, the stress of the notched sample dropped to a certain value and was almost constant. The time it takes for the stress to decrease to 1/e of the initial stress is defined as the relaxation time. As shown in Figure S10, the relaxation time of SE×1-KGW was about 1070 s, while the stress of P-KGW decreased quickly from 1.09 MPa to 0.77 MPa within 0-500 s and varied little with the extension of time. After reaching 3500 s, the stress was kept at about 0.66 MPa. Therefore, the relaxation time of P-KGW cannot be obtained under the test condition. And this result verified the good elasticity of P-KGW, compared with control samples, indicating that hot-pressing could produce robust hydrogen bond network which can maintain stress well. What's more, as shown in Figure S11 and Figure 2g, the fracture energy of SE×1-KGW, SE×2-KGW, A-KGW, P-KGW were 17.73, 19.33, 28.09, 43.44 kJ/m^2, respectively, and P-KGW 's fracture energy was 2.45, 2.25 and 1.55 times that of other three ICOHs, respectively. High fracture energy can provide a security guarantee for the long-term stability of the mechanical properties of samples. Defects or micro-cracks may be formed in gel materials during repeated deformations, and thus the fatigue resistance of the notched ICOHs is more important. The single notch method was used to quantitatively determine the fatigue threshold of ICOHs. The fatigue thresholds of SE×1-KGW, SE×2-KGW, A-KGW and P-KGW were 495, 747, 417 and 1213 J/m^2, respectively (Figure 2h-i, Figure S12). P-KGW had the highest fatigue threshold and were tested for 30 000 cycles at an energy release rate of 1213 J/m^2. The photos taken showed that no crack propagation was observed during 10000th and 30000th cycles, demonstrating its excellent resistance to crack propagation (Figure S13). The excellent antifatigue performance laid the foundation for the long-term and reliable sensing of the ICOH strain sensors in practical applications. Figure 2j

summarized the mechanical properties of different ICOHs, and the tensile strength, modulus, fracture energy and fatigue threshold of P-KGW were superior to those of other control samples. The mechanical properties of P-KGW were also compared with those of other organohydrogels reported in the literatures and showed prominent advantages in the comprehensive mechanical performance (Figure 2k-l).

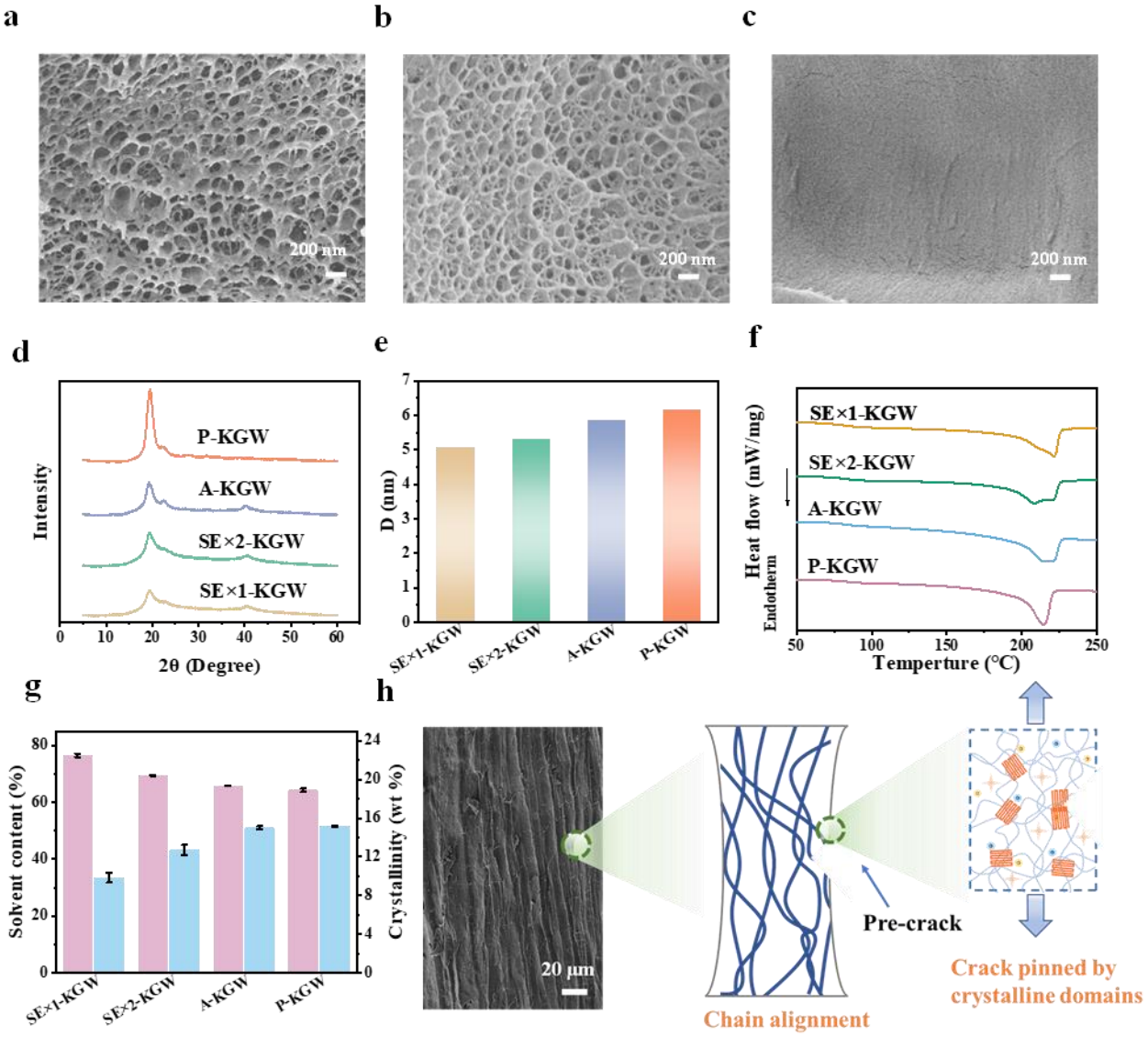

Figure 3. Structure characterization of different ICOHs. SEM images of (a) SE×1-KGW, (b) SE×2-KGW and (c) P-KGW. (d) XRD patterns and (e) summary of crystal size calculated by the XRD pattern. (f) DSC thermographs and (g) summary of solvent content and crystallinity of ICOHs in wet state calculated by DSC tests. (k) Scheme for the strengthening, toughening and fatigue resistance mechanism. The inset SEM image shows the aligned structure of P-KGW stretched by 100%.

All of ICOHs exhibited transparency, and P-KGW showed the highest transparency of about 90% (Figure S14). The high transparency reflected the formation of uniform and regular crystalline domains inside ICOHs after solvent exchange and hot-pressing, because uniform small sized crystals can effectively enhance light refraction and reduce light scattering, thereby improving the transparency of samples. SE×1-KGW and SE×2-KGW showed a uniform and densely porous structure with diameter of about 200 nm (Figure 3a-b). Compared with SE×2-KGW, the pore size of A-KGW was further reduced (Figure S15). At the same time, hot-pressing greatly densified the polymeric network of the

organohydrogels, and the porous structure almost disappeared inside P-KGW (Figure 3c). On one hand, A-KGW presented a rough fracture surface with nanosized humps and pores, and these pores may become defects inside organohydrogels and hence the weak points during the stretching. On the other hand, P-KGW exhibited a more densified polymeric network that can effectively deconcentrate stress and prevent crack propagation, greatly improving the mechanical properties including the tensile strength, fracture energy and fatigue threshold.

PVA is a typical semi-crystalline polymer. XRD was used to evaluate the crystalline performance of ICOHs. A wide and distinct diffraction peak of 19.6° was observed in all ICOHs and belonged to the (101) reflecting surface of PVA crystals (Figure 3d). Among them, P-KGW had the largest peak intensity, indicating hot-pressing improved the crystallinity as well as the growth of crystal size (Figure 3e)[37-39]. The crystalline behavior of ICOHs was also studied by DSC. The crystallinity of ICOHs in dry state and swelling state was calculated based on their melt enthalpies of the DSC curves. The results showed that there was little difference in crystallinity for ICOHs in the dry state, and the crystallinity was higher than 40 wt % (Figure 3f-g, Figure S16). However, their liquid (glycerol/water) content was different, and hence the crystallinity in the swelling state showed a great difference. The crystallinity of A-KGW and P-KGW in the swelling state reached ~15 wt %, higher than that of SE×1-KGW (about 10 wt %) and SE×2-KGW (about 13 wt %). The formation of a large number of crystals in P-KGW was conducive to the construction of a more uniform and compact polymer network and thus the enhancement of mechanical properties.

PVA, glycerol, and water all have very strong and abundant hydrogen bond interactions, and the changes of hydrogen bond can be verified from the rheological behavior of ICOHs. Both storage modulus (G') and loss modulus (G'') remained stable from 0 to 200 s, and ICOHs behaved like a solid with the storage modulus always one order of magnitude higher than the lose modulus (Figure S17). Among them, G' of P-KGW was the highest, exhibiting the strongest hydrogen bond network structure [40, 41]. Figure S18 showed the curve of G' and G'' as a function of shear strain (0.01~100%). When the shear strain was larger than 1%, G' decreased while G'' increased with the increase of shear strain. However, G' was still higher than G'', which proved that the destruction and reconstruction of the hydrogen bond network were in the dynamic equilibrium stage. The intersection between G' and G'' occurred at around 1~10%, after which G' was smaller than G''. A large number of hydrogen bonds were broken at such high shear strain, making ICOHs viscous.

The mechanism of strengthening, toughening and fatigue resistance of ICOHs in this study is schematically illustrated in Figure 3h. Hot pressing takes advantages of both wet-annealing and pressing that can fully adjust macromolecular conformation and promote the macromolecular chain aggregation and densification of polymeric network. Moreover, the solvent exchange and hot-pressing can reduce defects inside ICOHs and hence densify the polymeric network, where the stress can be deconcentrated. The numerous rigid crystalline domains bear the loading, while the entangled macromolecular chains in the amorphous regions provide large deformation capability. It is worth noting that the aligned structure with fiber bundles is present during stretching and can effectively blunt the crack propagation through the fiber bridging. Furthermore, the crystals as crosslinking points can pin the macromolecular chains and hence prevent the crack growth to a great degree. Finally, the slippage of molecular chains and damage of the hydrogen bonds also consume a large amount of energy. Based on the synergy of the hierarchical structures, P-KGW possesses excellent mechanical properties.

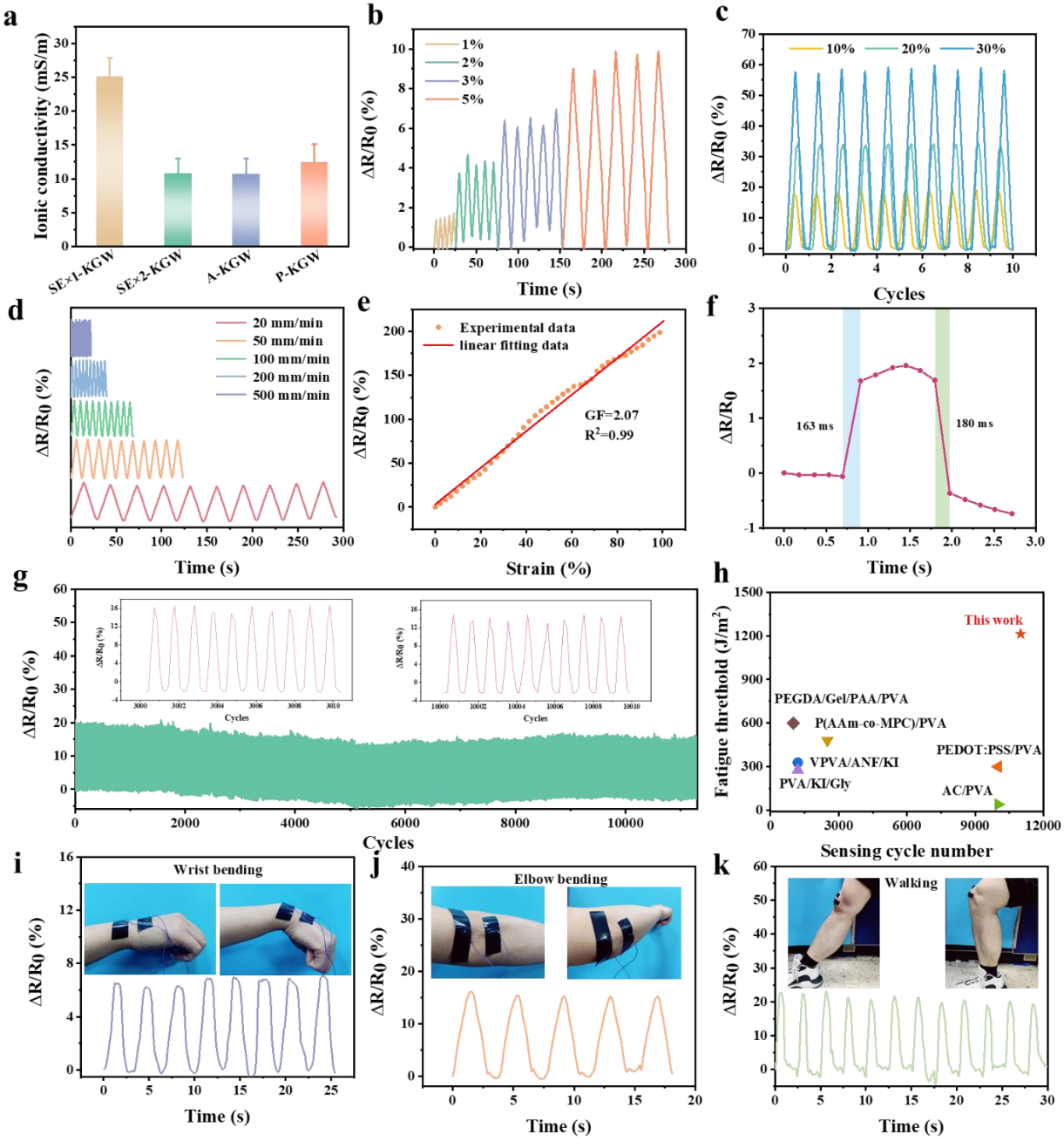

Figure 4. Strain sensing performance of P-KGW. (a) Ionic conductivity of different ICOHs. Relative resistance changes ($\Delta R/R_0$) under (b) small strain (1-5%) and (c) large strains (10-30%). (d) $\Delta R/R_0$ under different tensile rates at a fixed strain of 20%. (e) linear fitting of $\Delta R/R_0$ *versus* tensile strain for calculation of the gauge factor. (f) Response and recovery time at 1% strain. (g) Cycling stability within 10 000 cycles at a strain of 10%. (h) Comparison of the PVA gel strain sensors by fatigue threshold and sensing robustness (VPVA-ANF-KI [24], PVA/KI/Gly [42], P(AAm-co-MPC)/PVA [43], PEGDA/Gel/PAA/PVA [44], PEDOT:PSS-PVA [45], AC-PVA [46]) . Monitoring of human movement for (i) Wrist bending, (j) Elbow bending and (k) Walking.

As mentioned, the ionic conductivity of ICOHs increased with KI concentration. At a fixed KI concentration, the ionic conductivity was strongly related with the polymeric network that affected the ion movement in the organohydrogel. As shown in Figure 4a and Figure S19, SE×1-KGW possessed

the highest ionic conductivity of 25.01 mS/m, because its loose and porous structure was beneficial to the ion movement, and P-KGW exhibited a slightly higher conductivity (12.5 mS/m) than SE×2-KGW and A-KGW. In a seven-day open environment, P-KGW showed a solvent retention rate of up to 98%, higher than 94, 94 and 95% of SE×1-KGW, SE×2-KGW, and A-KGW, respectively (Figure S20).

Benefiting from the superior mechanical properties, satisfactory ionic conductivity and environment tolerance, ICOHs were good candidates for high-performance strain sensors. As shown in Figure 4b and c, P-KGW showed stable resistance response signals to both small strain (as low as 1%) and large strain. During the stretching, the ion transport path inside ICOHs was narrowed, and the ion movement became difficult, resulting in the increase of the resistance. The sensitivity can be described by response intensity (R_I), i.e., the maximum relative resistance change ($\Delta R/R_0$, ΔR and R_0 refer to the resistance change and initial resistance) under a given strain. Obviously, R_I was proportional to the applied strain and reached ~ 0.6 at the strain of 30%. Furthermore, with a fixed strain of 20%, R_I remained almost the same at different stretching rates (from 20 to 500 mm/min), and the strain sensor responded quickly with consistent and stable R_I even at a high rate of 500 mm/min (Figure 4d). The results indicated that the reliable and stable output sensing signals with the same response intensity can be obtained, regardless of the frequency of mechanical deformations. It was also found that $\Delta R/R_0$ displayed almost linear change with the strain (0-100%), and the strain sensitivity was quantitatively described by the gauge factor (GF) that can be obtained from the slope of the fitted straight line, and GF of P-KGW strain sensor was calculated to 2.07 (Figure 4e). Apart from GF, the response time was a key factor evaluating the strain sensing performance. At the stretching rate of 500 mm/min, the response time of the strain sensor at 1% strain was 163 ms and the recovery time was 180 ms, which verified the quickly response ability (Figure 4f).

Figure 4g showed $\Delta R/R_0$ of the P-GHK strain sensor during 10 000 repeated stretching and releasing cycles with the tensile strain and tensile rate of 10% and 500 mm/min, respectively. In such long cycles, the resistance quickly increased during stretching while decreased to its original value after the releasing, and no obvious sensing hysteresis was observed. The sensing curves were not different from each other with unchanged response intensity, as verified from randomly selected ten cycles from the whole strain sensing test (Figure 4g). The long-term stability of the strain sensing signals was attributed to the outstanding anti-drying capability, originating from the rich hydrogen

bonds between glycerol and water. In addition, the excellent mechanical properties including the high strength, toughness and fatigue resistance endowed the P-KGW strain sensor with sufficient resilience and structure stability during multiple stretching and releasing cycles. Compared with other reported of PVA gel-based strain sensors, P-KGW in this study showed remarkable advantages in fatigue thresholds and cyclic stability (Figure 4h).

The excellent strain sensing performance makes it possible for ICOHs to monitor human motions. As a proof of concept, the P-KGW sensor was attached to different joints of human body including the wrist, elbow and knee, respectively. When the joints were bent, the strain sensors were stretched with the increase of the resistance, and the periodic and stable sensing signals were observed during the repeated bending. R_I was determined by the amplitude of joint bending. For example, R_I was only ~ 0.06 for wrist bending, while it was greatly improved to 0.15 and 0.22 for elbow and knee bending, respectively (Figure 4i-k). The strain sensor can also accurately distinguish different angles of joint bending. For instance, when the finger was bent at different angles and stayed for a few seconds, the strain sensor could respond quickly (Figure S21 (a)). Moreover, the relative resistance changes showed a plateau when the finger kept fixed. When grasping oranges and apples, the finger was bent at different angles, and different R_I was obtained (Figure S21 (b)). These results proved that the P-KGW strain sensor was able to distinguish clearly different human movements, displaying the powerful recognition capability.

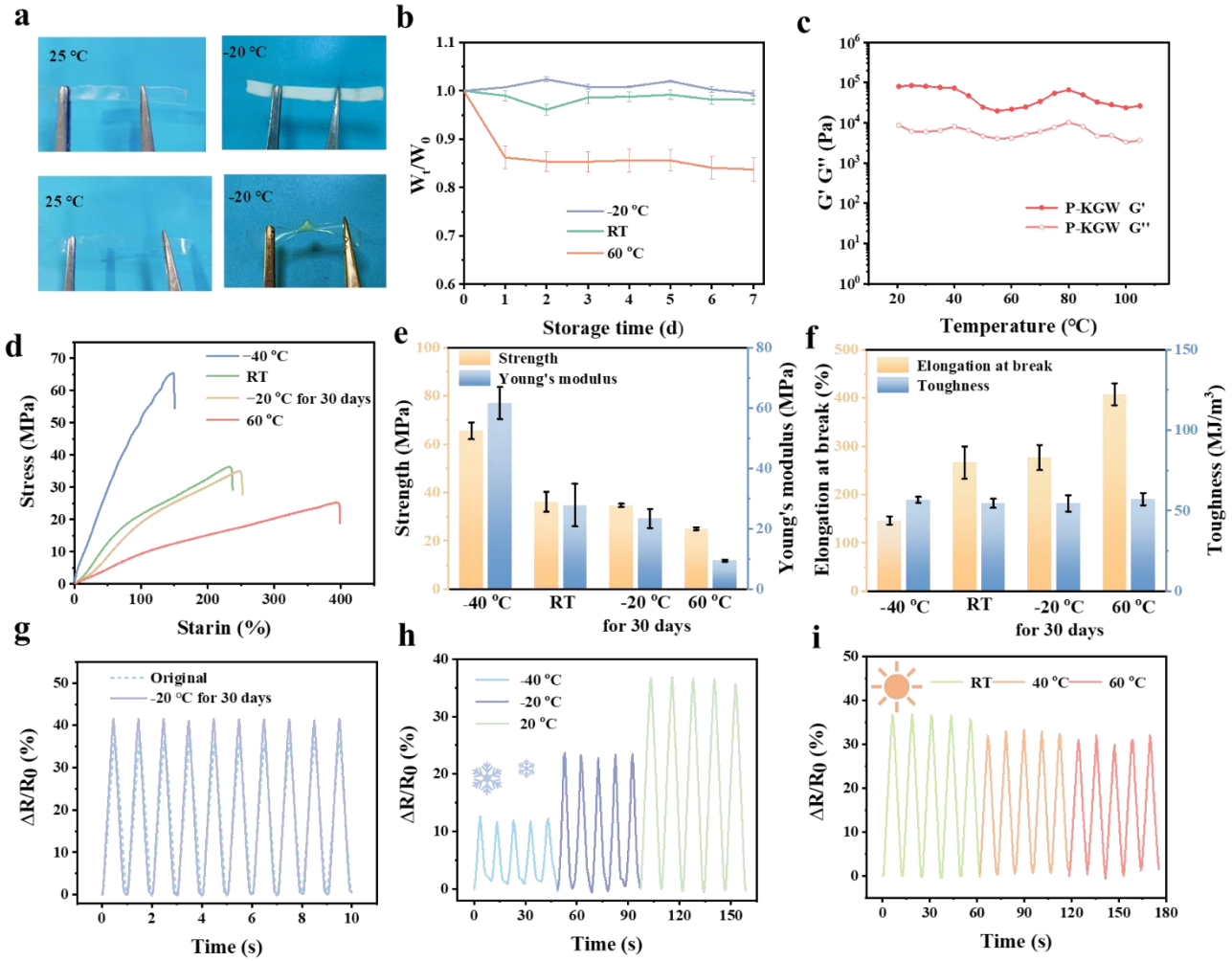

Figure 5. Environmental tolerance and durability of P-KGW. (a) Photographs of hydrogels and P-KGW at 25 and −20 ℃. (b) Mass change with the time at different temperatures. (c) *G'* and *G''* with a temperature sweep in the range of 20 ℃ to 100 ℃. (d) Tensile stress-strain curves at different temperatures, and summary of (e) tensile strength and Young's modules and (f) elongation at break and toughness. Strain sensing performance of P-KGW (g) after stored at −20 ℃ for 30 days, (h) with the decrease of the temperature to −20 and −40 °C, and (i) with the increase of the temperature to 40 and 60 °C. Note that the strain sensors were stretched and released for a few cycles with a tensile strain of 20% and a tensile rate of 50 mm min^{-1}.

The PVA hydrogel turned to white and lost flexibility at −20 ℃, while P-KGW remained transparent and could be twisted at such a low temperature (Figure 5a), exhibiting freezing resistance. From the quality change of P-KGW at different temperatures (Figure 5b), it can be found that the mass almost kept at its original value with the quality retention rate of 98% and 99%, respectively at −20 ℃ and room temperature during the 7 days exposure. Even at a high temperature of 60 ℃, the mass of P-KGW dropped by 14% after the first day and remained almost unchanged during the following six days. Moreover, as showed in Figure S22, no freezing peak was observed when P-KGW were cooled from 0 ℃ to -65 ℃ and an inconspicuous peak appears at -62 ℃, confirming its freezing resistance.

Glycerol was served as an antifreeze agent in P-KGW, and the abundant hydrogen bonds between glycerol and water significantly decreases the vapor pressure of water, making evaporation difficult, which delays or prevents the formation of solvent crystals even at -60 ℃. *G'* and *G''* of P-KGW were stable from 20 to 100 ℃, indicating excellent thermal stability and liquid retention capability (Figure 5c). The detailed information about the mechanical properties of P-KGW at different temperatures were shown in Figure 5d-f. After stored at -20 ℃ for 30 days, P-KGW maintained its mechanical properties without decline of tensile strength and elongation at break. On the other hand, temperature indeed influenced the mechanical properties of P-KGW. The decrease of the temperature can increase the tensile strength while reduce the elongation at break. The tensile strength of P-KGW decreased from 36.1 MPa at room temperature to 25.0 MPa at 60 ℃, while it was significantly enhanced to 65.5 MPa when the ambient temperature dropped to −40 ℃ (Figure S23). It was worth noting that the toughness was maintained at ~ 55 MJ/m^3, regardless of the temperature. These results demonstrated the excellent environmental tolerance of P-KGW, making it promising to work in various extreme environments. In addition, sensing properties of P-KGW were investigated. As expected, P-KGW after storage at −20 ℃ for 30 days exhibited nearly identical strain sensing behavior, and the cyclic sensing curves almost overlapped with those of the pristine samples (Figure 5g). However, R_I at low temperature and high temperature was completely different, which was similar with the influence of the temperature on mechanical properties. In a low temperature environment, R_I decreased with the decrease of temperature. R_I decreased largely from 0.37 at room temperature to 0.12 at −40 ℃ (Figure 5h). Nevertheless, R_I was almost consistent under high temperatures (Figure 5i). Due to environment tolerance (such as freezing and drying resistance) and superior mechanical performance, P-KGW can maintain flexibility and work effectively under various extreme environments.

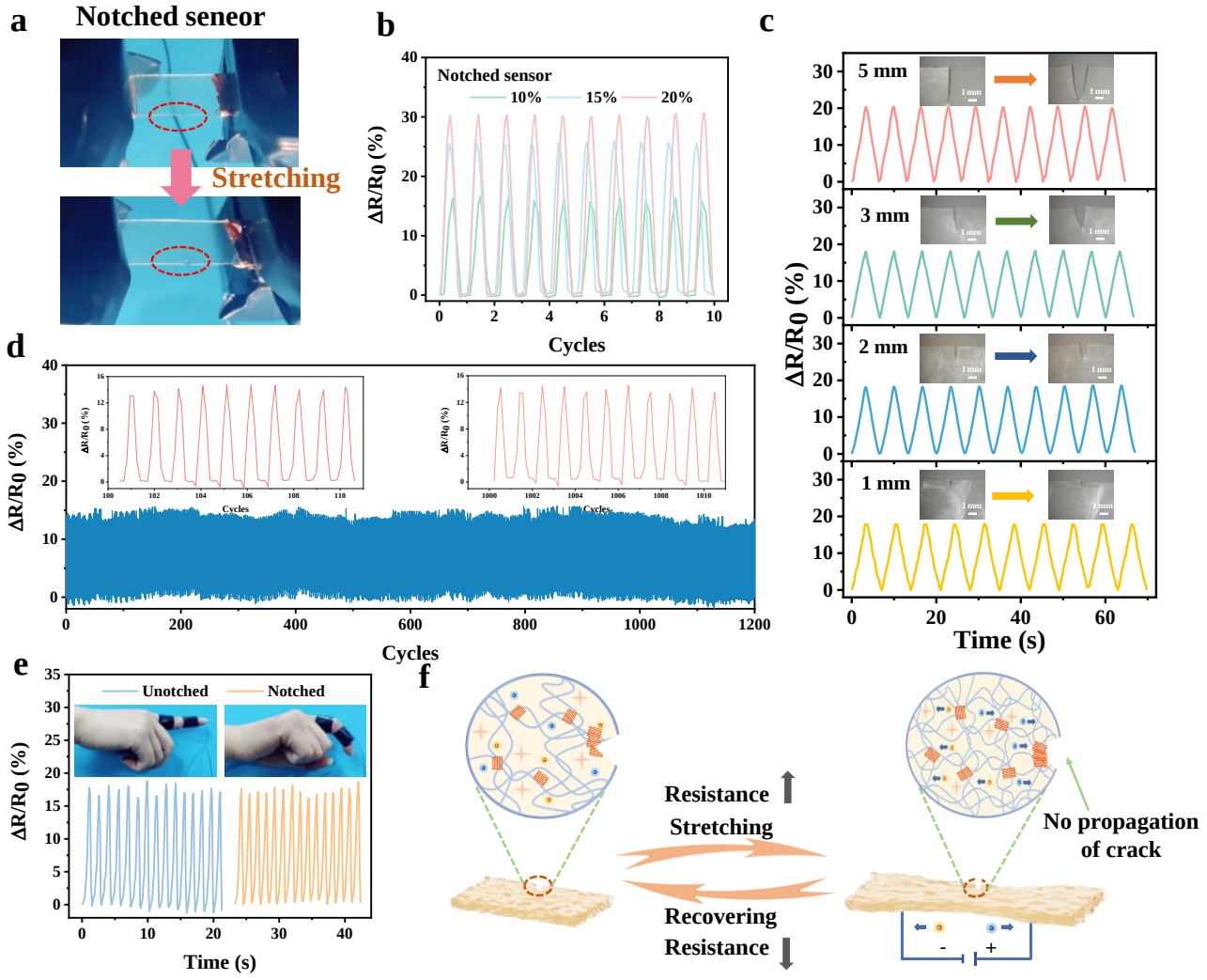

Figure 6. Flaw insensitive strain sensing performance of P-KGW. (a) Photographs of notched strain sensors before and after stretching. (b) $\Delta R/R_0$ of notched strain sensors at different tensile strains. (c) $\Delta R/R_0$ of notched strain sensors with different notch lengths under 10% tensile strain. (d) Cycling stability of notched strain sensors within 1200 cycles at a strain of 10%. (e) Comparison of $\Delta R/R_0$ of finger bending for the notched and unnotched sensor. (j) Sensing mechanism of notched strain sensors during stretching and recovery process.

P-KGW had excellent crack propagation resistance and its fatigue threshold was higher than that of most other gel-based sensors reported. This unique merit is especially desirable and important, because it can prevent the propagation of microcracks or defects generated during multiple deformations and hence ensure reliable sensing signal output. A notch of about 1 mm in length was made in the middle of P-KGW, and strain sensing tests of the notched samples were performed (Figure 6a). Figure 6b showed $\Delta R/R_0$ of the notched strain sensor under different tensile strains. Similar with the unnotched sample, R_I was proportional to the tensile strain, and increased from 0.17 to 0.30 with the increase of the strain from 10% to 20%. As shown in Figure 6c, $\Delta R/R_0$ of the notched strain sensor

with different notch lengths under the same strain was almost the same. The sensing signals of notched strain sensor remained stable during the 1200 stretching cycles (Figure 6d), and the strain sensing curves randomly selected 100-110 and 1000-1010 cycles resemble each other, demonstrating satisfactory fatigue resistance and durability for the sensing performance. When used for body motion monitoring, the notched P-KGW can make a fast and stable response to finger bending and displayed almost the same sensing signals with the unnotched sample (Figure 6e). The anti-fatigue strain sensors with flaw insensitivity can work normally even in the presence of cracks, and showed promising applications in high-performance flexible and wearable electronics. Similar to conventional ion-conducting hydrogels, when ICOHs were stretched, the stretched gel network was denser, and the narrowing of ion channels made it difficult for free ions to move, resulting in increased resistance (Figure 6f). Fortunately, P-KGW possessed outstanding anti-fatigue capability, and the notch kept un-propagated during the cyclic stretching. As a result, the notched P-KGW strain sensor output the stable and periodical signals almost the same with those of the unnotched sample, regardless of the notch length.

3. Conclusion

In this work, strong, transparent and anti-fatigue ICOHs were prepared based on the strategy of solvent exchange and hot pressing. ICOHs possess densified polymeric network, numerous crystalline domains and hydrogen bonds and hence show excellent mechanical properties. The tensile strength, toughness, fracture energy and fatigue threshold of P-KGW can reach 36.12 ± 4.15 MPa, 54.57 ± 2.89 MJ/m^3, 43.44 ± 8.54 kJ/m^2 and 1212.86 ± 57.20 J/m^2, respectively. What's more, environmentally stable ICOHs exhibit freezing resistance and thermal stability due to the abundant hydrogen bonding between glycerol and water. As a strain sensor, P-KGW shows a quick response and excellent cyclability (10 000 cycles). Furthermore, ICOHs with ultra-high fatigue threshold allow the notched strain sensor to work normally with the stable and reliable sensing signal output. The unique flaw-insensitive strain sensing makes ICOHs promising in the field of high performance and durable electronics.

4. Experimental Section

Materials: Poly(vinyl alcohol) (PVA-1799, 98-99% hydrolyzed) was supplied from Macklin. Glycerol and glutaraldehyde solution (50 vol%) were bought from Aladdin. Potassium iodide (KI) and hydrochloric acid (HCI) were received from Sinopharm Chemical Reagent Co. Ltd. All the chemicals were used without further purification.

Fabrication of Organogels: PVA solid powders (3 g) were added to water (17 g) and the mixture was heated in an oil bath at 100 ℃ for 5 h to obtain a homogeneous solution. The concentration of PVA was 15 wt %. PVA/water solutions were poured into Teflon molds and defoamed by standing at room temperature. Then, the molds were transferred to glycerol solutions at room temperature for 48 h, and glycerol was replaced every 6 h. Finally, the PVA/glycerol organogels were obtained.

Fabrication of Ionically Conductive Organohydrogels: The organogels were hot-pressed at different temperatures for 15 min under a fixed pressure of 10 MPa. Finally, the hot-pressed organogels were immersed in KI/glycerol/water with the weight ratio of glycerol to water of 3:1 for 48 h to obtain the organohydrogels. The ionically conductive organohydrogels were represented by P_x-K_yGW., where *x* referred to the temperature of hot pressing, and *y* was the weight concentration of KI dissolved in the glycerol/water solution. It should be noted that the glycerol/water solution with KI of 30% was named KGW. For comparison, three control group samples were also prepared. 1)The PVA/water solutions were poured into the Teflon molds and directly immersed in KI/glycerol/water to obtain organohydrogels represented by SE×1-KGW. 2) Organogels were immersed in KI/glycerol/water solution without hot-pressing to obtain organohydrogels represented by SE×2-KGW. 3) The organogels were wet-annealed at 120 ℃ for 15 min without pressing and then immersed in KI/glycerol/water solution to obtain organohydrogels represented by A-KGW. 4) PVA was dissolved in glycerol at 150 ℃ for 3 h, and then the PVA/glycerol solution was cooled to room temperature and gradually formed a white opaque organogel. The organogel was dipped into KI/glycerol/water for 48 h to obtain organohydrogels represented by HC-GHK.

Author contributions

Yuqing Wang and Zhanqi Iiu: Methodology, Data curation, Formal Analysis and writing original draft; Yuntao Liu, Jun Yan, Haidi Wu and Hechuan Zhang: review and editing; Huamin Li and Junjie Wang:

Methodology, formal analysis; Huaiguo Xue, Ling Wang, Yongqian Shi, Longcheng Tang and Pingan Song: Writing-review & editing; Jiefeng Gao: Conceptualization, Resources, Writing-Review & Editing and Funding acquisition.

Supporting Information

Material characterization and related performance testing.

Acknowledgement

This work was financially supported by Natural Science Foundation of China (No. 52303069, 51873178), Qing Lan Project of Yangzhou University and Jiangsu Province, High-end Talent Project of Yangzhou University.

Conflict of Interest

The authors declare no conflict of interest.

References

1. Kuzina M A, Kartsev D D, Stratonovich A V and Levkin P A. *Adv. Funct. Mater.* 2023, **33**, 2301421.
2. Zhang Z and Hao J. *Adv. Colloid Interface Sci.* 2021, **292**, 102408.
3. Dong X, Guo X, Liu Q, Zhao Y, Qi H and Zhai W. *Adv. Funct. Mater.* 2022, **32**, 2203610.
4. Zhu L, Xu J, Song J, Qin M, Gu S, Sun W and You Z. *Sci. China Mater.* 2022, **65**, 2207-2216.
5. Tang J, He Y, Xu D, Zhang W, Hu Y, Song H, Zhang Y, Chen Y M, Yang Y and Zhang K. *npj Flex. Electron.* 2023, **7**, 28.
6. Wen J, Wu Y, Gao Y, Su Q, Liu Y, Wu H, Zhang H, Liu Z, Yao H, Huang X, Tang L, Shi Y, Song P, Xue H and Gao J. *Nano-Micro Lett.* 2023, **15**, 174.
7. Yu D, Yi J, Zhu S, Tang Y, Huang Y, Lin D and Lin Y. *Adv. Funct. Mater.* 2024, **n/a**, 2307566.
8. Bi D, Qu N, Sheng W, Lin T, Huang S, Wang L and Li R. *ACS Appl. Mater. Interfaces*. 2024, **16**, 11914.
9. Wu H, Wu Y, Yan J, Xiao W, Wang Y, Zhang H, Huang X, Xue H, Wang L, Tang L, Mai Y and Gao J. *Chem. Eng. J.* 2024, **488**, 150963.
10. Zhuo F, Zhou J, Liu Y, Xie J, Chen H, Wang X, Luo J, Fu Y, Elmarakbi A and Duan H. *Adv. Funct. Mater.* 2023, **33**, 2308487.
11. Wei Y, Xiang L, Ou H, Li F, Zhang Y, Qian Y, Hao L, Diao J, Zhang M, Zhu P, Liu Y, Kuang Y and Chen G. *Adv. Funct. Mater.* 2020, **30**, 2005135.
12. Hou X, Zhang Q, Wang L, Gao G and Lü W. *ACS Appl. Mater. Interfaces*. 2021, **13**, 12432-12441.
13. Wang J, Ding Z, Yang J, Cheng J, Huang C, Xiong C, Cai X, You L and Wang S. *J. Mater. Chem. C*. 2023, **11**, 554-573.
14. He H, Li H, Pu A, Li W, Ban K and Xu L. *Nat. Commun.* 2023, **14**, 759.
15. Feig V R, Tran H, Lee M and Bao Z. *Nat. Commun.* 2018, **9**, 2740.
16. Chong J, Sung C, Nam K S, Kang T, Kim H, Lee H, Park H, Park S and Kang J. *Nat. Commun.* 2023, **14**, 2206.
17. Song J, Chen S, Sun L, Guo Y, Zhang L, Wang S, Xuan H, Guan Q and You Z. *Adv. Mater.* 2020, **32**, 1906994.

18. Liu J, Chen Z, Chen Y, Rehman H U, Guo Y, Li H and Liu H. *Adv. Funct. Mater.* 2021, **31**, 2101464.
19. Lyu J, Zhou Q, Wang H, Xiao Q, Qiang Z, Li X, Wen J, Ye C and Zhu M. *Adv. Sci.* 2023, **10**, 2206591.
20. Ye Y, Zhang Y, Chen Y, Han X and Jiang F. *Adv. Funct. Mater.* 2020, **30**, 2003430.
21. Niu Y, Liu H, He R, Luo M, Shu M and Xu F. *Small*. 2021, **17**, 2101151.
22. Zheng B, Zhou H, Wang Z, Gao Y, Zhao G, Zhang H, Jin X, Liu H, Qin Z, Chen W, Ma A, Zhao W and Wu Y. *Adv. Funct. Mater.* 2023, **33**, 2213501.
23. Feng Y, Liu H, Zhu W, Guan L, Yang X, Zvyagin A V, Zhao Y, Shen C, Yang B and Lin Q. *Adv. Funct. Mater.* 2021, **31**, 2105264.
24. Wu Y, Zhang Y, Liao Z, Wen J, Zhang H, Wu H, Liu Z, Shi Y, Song P, Tang L, Xue H and Gao J. *Mater. Horiz.* 2024, **11**, 1272-1282.
25. Chen H, Huang J, Liu J, Gu J, Zhu J, Huang B, Bai J, Guo J, Yang X and Guan L. *J. Mater. Chem. A*. 2021, **9**, 23243-23255.
26. Xu L, Gao S, Guo Q, Wang C, Qiao Y and Qiu D. *Adv. Mater.* 2020, **32**, 2004579.
27. Wu Y, Xing W, Wen J, Wu Z, Zhang Y, Zhang H, Wu H, Yao H, Xue H and Gao J. *Polymer*. 2023, **267**, 125661.
28. Zhang H, Tang N, Yu X, Li M-H and Hu J. *Adv. Funct. Mater.* 2022, **32**, 2206305.
29. Cheng Y, Ren X, Gao G and Duan L. *Carbohydr. Polym.* 2019, **223**, 115051.
30. Zha X-J, Zhang S-T, Pu J-H, Zhao X, Ke K, Bao R-Y, Bai L, Liu Z-Y, Yang M-B and Yang W. *ACS Appl. Mater. Interfaces*. 2020, **12**, 23514-23522.
31. Zou J, Jing X, Chen Z, Wang S-J, Hu X-S, Feng P-Y and Liu Y-J. *Adv. Funct. Mater.* 2023, **33**, 2213895.
32. Guo B, Yao M, Chen S, Yu Q, Liang L, Yu C, Liu M, Hao H, Zhang H, Yao F and Li J. *Adv. Funct. Mater.* 2024, **n/a**, 2315656.
33. Li N, Yu Q, Duan S, Du Y, Shi X, Li X, Jiao T, Qin Z and He X. *Adv. Funct. Mater.* 2024, **34**, 2309500.
34. Guo R, Bao Y, Zheng X, Zhang W, Liu C, Chen J, Xu J, Wang L and Ma J. *Adv. Funct. Mater.* 2023, **33**, 2213283.
35. Bai R, Yang Q, Tang J, Morelle X P, Vlassak J and Suo Z. *Extreme Mech. Lett.* 2017, **15**, 91-96.
36. Si M, Jian X, Xie Y, Zhou J, Jian W, Lin J, Luo Y, Hu J, Wang Y-J, Zhang D, Wang T, Liu Y, Wu Z L, Zheng S Y and Yang J. *Adv. Energy Mater.* 2024, **14**, 2303991.
37. Wan H, Wu B, Hou L and Wu P. *Adv. Mater.* 2024, **36**, 2307290.
38. Liang X, Chen G, Lei I M, Zhang P, Wang Z, Chen X, Lu M, Zhang J, Wang Z, Sun T, Lan Y and Liu J. *Adv. Mater.* 2023, **35**, 2207587.
39. Liang X, Chen G, Lin S, Zhang J, Wang L, Zhang P, Wang Z, Wang Z, Lan Y, Ge Q and Liu J. *Adv. Mater.* 2021, **33**, 2102011.
40. Song G, Zhao Z, Peng X, He C, Weiss R A and Wang H. *Macromolecules*. 2016, **49**, 8265-8273.
41. Wu Y, Zhang Y, Wu H, Wen J, Zhang S, Xing W, Zhang H, Xue H, Gao J and Mai Y. *Adv. Mater.* 2023, **35**, 2210624.
42. Wang Y, Wu Y, Liu Y, Wu H, Xiao W, Zhang H, Huang X, Zhang J, Xue H-G and Gao J-f. *ACS Mater. Lett.* 2024, **6**, 1140-1150.
43. Zhao C, Dong Z, Guo M, Liu L, Wu Y, Li Y, Xiang D, Li H, Lai J and Wang L. *Polymer Engineering & Science*. 2022, **62**, 2532-2540.
44. Liu J, Zhang P, Wei H, Lu Z and Yu Y. *Adv. Funct. Mater.* 2022, **32**, 2107732.

45. Zhang Z, Chen G, Xue Y, Duan Q, Liang X, Lin T, Wu Z, Tan Y, Zhao Q, Zheng W, Wang L, Wang F, Luo X, Xu J, Liu J and Lu B. *Adv. Funct. Mater.* 2023, **33**, 2305705.
46. Wang L, Zhang Z, Cao J, Zheng W, Zhao Q, Chen W, Xu X, Luo X, Liu Q, Liu X, Xu J and Lu B. *Polymers*. 2023, **15**, 90.